Article

Not peer-reviewed version

Bicarbazole-Benzophenone Based Twisted D-A-D Derivatives as Blue Emitters for Highly Efficient Fluorescent OLEDs

Dovydas Blazevicius , Iram Siddiqui , Prakalp Gautam , Gintare Krucaite , Daiva Tavgeniene , Mangey Ram Nagar , Krishan Kumar , Subrata Banik , Jwo-Huei Jou * , Saulius Grigalevicius *

Posted Date: 9 November 2023

doi: 10.20944/preprints202311.0596.v1

Keywords: Donor-acceptor-donor (D-A-D) derivatives; blue organic light emitting diode (OLED); high efficiency; blue emission; thermal analysis

Article

Bicarbazole-Benzophenone Based Twisted D-A-D Derivatives as Blue Emitters for Highly Efficient Fluorescent OLEDs

Dovydas Blazevicius [1,§], Iram Siddiqui [2,§], Prakalp Gautam [2], Gintare Krucaite [1], Daiva Tavgeniene [1], Mangey Ram Nagar [2], Krishan Kumar [3], Subrata Banik [4], Jwo-Huei Jou [2,*] and Saulius Grigalevicius [1,*]

[1] Department of Polymer Chemistry and Technology, Kaunas University of Technology, Radvilenu Plentas 19, LT50254 Kaunas, Lithuania
[2] Department of Materials Science and Engineering, National Tsing Hua University, No. 101, Section 2, Guangfu Rd., East District, Hsinchu, Taiwan, 30013
[3] School of Chemical Sciences, IIT Mandi, Himachal Pradesh 175005, India
[4] Department of Chemistry, School of Chemical and Biotechnology, SASTRA Deemed University, Thanjavur 613401, Tamil Nadu, India.
§ These authors contributed equally to this work.
* Correspondence: authors e-mail: saulius.grigalevicius@ktu.lt and jjou@mx.nthu.edu.tw

Abstract: Organic light-emitting diodes (OLEDs) have ushered in a technological revolution with their remarkable impact on diverse sectors of our daily lives. These versatile devices known for their outstanding display and lighting capabilities, have become indispensable components in various industries including smartphones, tablets, televisions, and automotive applications. This paper delves into the development of a group of twisted donor-acceptor-donor (D-A-D) derivatives incorporating bicarbazole and benzophenone structures for potential use as blue emitters in OLEDs. The synthesized compounds, namely DB14, DB23 and DB29, were designed with various alkyl side chains to enhance their film forming properties as for blue emitters. Characterization and evaluation of these derivatives included photophysical, electrochemical, thermal, and electroluminescent analysis. Some of the OLED devices incorporating these emitters demonstrated promising performance with maximum current efficiency (CE_{max}) of 2.6 cd/A and external quantum efficiency (EQE_{max}) of 5.3%. Notably, the DB23 emitter exhibited the highest EQE among all devices. The study also emphasizes the influence of host-guest energy transfer, optimal doping concentrations, and molecular structures on device performance. This research not only contributes to the understanding of advanced OLED materials but also provides insights into designing efficient blue emitters for future display and lighting applications, thereby advancing the field of organic electronics.

Keywords: donor-acceptor-donor (D-A-D) derivatives; blue organic light emitting diode (OLED); high efficiency; blue emission; thermal analysis

1. Introduction

Ever since Nakamura and his colleagues pioneered blue light-emitting diodes (LEDs) [1–3], they have brought about a paradigm shift in our modern world. These LEDs have not only facilitated full-color displays but also revolutionized white lighting, profoundly shaping human existence [4,5]. At present, organic light-emitting diode (OLED) technology has emerged as a dominant force in both display and lighting applications. OLEDs are steadily advancing in terms of their performance, longevity and production processes [6,7]. Numerous companies are dedicating their efforts by creating and refining OLED materials with high purity and establishing top-notch manufacturing facilities. OLEDs have found their place across diverse sectors of the display industry, including television (TV), computers, smartphones, tablets, monitors, digital cameras, smartwatches, electric razors, PDAs, mp3/mp4 players, automobiles, and indoor and outdoor lighting [8]. In order to provide vivid full-color displays and energy-efficient lighting solutions, blue OLEDs are an essential

 doi:10.20944/preprints202311.0596.v1

technological component. Despite their significance, the development of blue OLEDs has posed persistent challenges owing to the inherent instability of blue-emitting materials [9]. Recent research efforts have resulted in notable progress in the domain of solution-processable host materials for blue OLEDs, offering promising avenues to overcome the efficiency limitations observed in conventional fluorescent OLEDs and reached nearly perfect internal quantum efficiency [9,10]. This research thrust encompasses a multifaceted approach to address key challenges in designing high-performance host materials, with a particular emphasis on optimizing efficiency, ensuring long-term stability and enabling solution-based fabrication processes [10]. Simultaneously, scientists and engineers have made noteworthy strides in the creation of novel organic emitters tailored for narrow-band deep blue OLEDs[11]. These emitters were engineered to deliver high efficiency, exceptional color purity, and a narrow emission bandwidth, addressing the demands of modern OLED technology [11]. Notably, these advancements also include the development of deep blue emitters characterized by rigid molecular structures and elevated triplet exciton energies, which contribute significantly to the overall performance of blue OLEDs [12,13]. As research continues to advance, the pursuit of innovative materials and tailored design strategies holds the promise of propelling blue OLED technology to even greater heights.[9–14] In this research article, we have designed a group of twisted D-A-D derivatives incorporating bicarbazole and benzophenone fragments that have been developed for potential use as blue emitters in OLEDs. These derivatives include 4,4'-bis(9'-butyl-[3,3']-bicarbazol-9-yl)benzophenone (DB14), 4,4'-bis(9'-{2-ethylhexyl}-[3,3']- bicarbazol-9-yl)benzophenone (DB23) and 4,4'-bis(9'-octyl-[3,3']-bicarbazol-9-yl)benzophenone (DB29). The compounds were designed with different alkyl side chains, which determine film forming and correspondingly emitting properties of the blue emitters. Some of the OLED devices based on the bicarbazole and benzophenone fragments containing D-A-D emitters demonstrated promising performance as compared with that of carbazole- benzophenone based emitters [15]. Specifically, one device exhibited the peak current efficiency (CE_{max}) of 2.6 cd/A and a peak external quantum efficiency (EQE_{max}) of 5.3%, producing a greenish-blue emission with a CIE_y coordinate of (0.22, 0.22).

2. Experimental Section

2.1. Instruments

Thermogravimetric analysis (TGA) was conducted utilizing a TGAQ50 instrument (Verder Scientific Haan, Haan, Germany). Both TGA and differential scanning calorimetry (DSC) profiles were recorded under a nitrogen atmosphere at a controlled heating rate of 10 °C/min. For differential scanning calorimetry (DSC) measurements, a Bruker Reflex II thermos-system (Bruker, Berlin, Germany) was employed. UV–visible spectroscopy was carried out using an HP-8453 diode array spectrometer (Agilent Technology Inc., Hachioji, Tokyo, Japan) to capture the absorption spectra of the compounds. Moreover, the Tauc plot was generated using the absorbance wavelength data. Photoluminescence (PL) spectra were captured utilizing the Aminco-Bowman Series 2 luminescence spectrometer (Agilent Technology Inc., Hachioji, Tokyo, Japan). For low-temperature PL (LTPL), a Hitachi F-7000 fluorescence spectrophotometer (Edinburgh Instruments Ltd., Livingston, UK) was employed. The LTPL measurements were performed at a temperature of 77K to ascertain the singlet energy of the compounds. Cyclic voltammetry (CV) experiments were conducted using the CH instrument CH1604A potentiostat (Annatech Co., Ltd., Taipei, Taiwan). The highest occupied molecular orbital (HOMO) levels were determined based on the results from the CV measurements. Time-resolved photoluminescence measurements were executed using an Edinburgh instrument spectrometer FLS980 (Edinburgh Instruments Ltd., Livingston, UK) to accurately determine the decay time of the compounds.

2.2. Synthesis and structure characterization of the materials

Carbazole (1), benzylbromide, bromoethane, 1-bromobutane, 1-bromohexane, 2-ethylhexylbromide, 1-bromooctane, $FeCl_3$, KOH, K_2CO_3, NaH, Na_2SO_4, 4,4‘-difluorobenzophenone,

Preprints (www.preprints.org) | NOT PEER-REVIEWED | Posted: 9 November 2023 doi:10.20944/preprints202311.0596.v1

chloroform, DMF and THF were purchased from Aldrich and used as received. 3,3′-Bicarbazole (2) was obtained by oxidation of carbazole using $FeCl_3$ as it was described earlier.

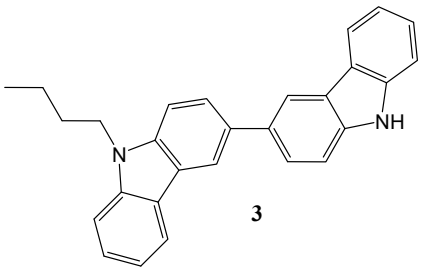

3

9-Butyl-9′H-3,3′-bicarbazole (**3**). 1-Bromobutane (0.82 g, 6.02 mmol) was added to a stirred solution of 3,3′-bicarbazole (**2**) (2.00 g, 6.02 mmol) in 50 ml of tetrahydrofuran. The mixture was heated to reflux, then potassium carbonate (1.66 g, 12.04 mmol) and powdered potassium hydroxide (2.02 g, 36.12 mmol) were added stepwise. The resulting mixture was left to react for 4h. After TLC control, the inorganic salts were filtered off and the product was purified by silica gel column chromatography using tetrahydrofuran/hexane (vol. ratio 1:5) as an eluent. Yield: 0.96 g (41%) of yellowish material. ^{1}H NMR (400 MHz, $CDCl_3$-d_6, δ, m.d.): 8.29 (s, 2H), 8.11-8.06 (m, 2H), 7.73-7.67 (m, 2H), 7.41-7.32 (m, 6H), 7.17 (t, 2H, J = 7.2 Hz), 4.29 (t, 2H, J = 7.2 Hz), 1.79 (quint, 2H, J = 7.2 Hz), 1.38-1.29 (m, 2H), 0.87 (t, 3H, J = 7.2 Hz). ^{13}C NMR (400 MHz, $CDCl_3$-d_6, δ, m.d.): 139.64, 138.56, 133.33, 125.94, 125.86, 125.72, 125.57, 124.00, 123.61, 123.43, 123.08, 120.51, 120.46, 119,51, 119.03, 119.00, 118.92, 118.82, 110.83, 110.77, 108.95, 108.86, 42.99, 31.25, 20.65, 13.97. MS (APCI$^+$, 20 V): 339.10 ([M+H], 100%).

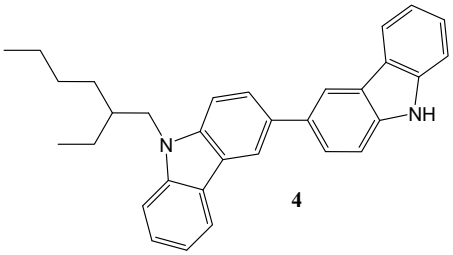

4

9-(2-Ethylhexyl)-9′H-3,3′-bicarbazole (**4**) was synthesized by a similar procedure that was described earlier. 2-Ethylhexylbromide (1.16 g, 6.02 mmol) was added to a stirred solution of 3,3′-bicarbazole (**2**) (2.00 g, 6.02 mmol) in 50 ml of tetrahydrofuran. The mixture was heated to reflux, then potassium carbonate (1.66 g, 12.04 mmol) and powdered potassium hydroxide (2.02 g, 36.12 mmol) was added stepwise. The resulting mixture was left to react for 4h. After TLC control, the inorganic salts were filtered off and the product was purified by silica gel column chromatography using tetrahydrofuran/hexane (vol. ratio 1:7) as an eluent. Yield: 1.28 g (48%) of yellowish material. ^{1}H NMR (400 MHz, $CDCl_3$-d_6, δ, m.d.): 8.47 (d, 2H, J = 7.2 Hz), 8.26 (d, 1H, J = 7.6 Hz), 8.23 (d, 1H, J = 7.6 Hz), 7.88 (d, 1H, J = 7.2 Hz), 7.84 (dd, 1H, J_1 = 8.4 Hz, J_2 = 1.6 Hz), 7.57-7.43 (m, 6H), 7.33 (t, 2H, J = 7.2 Hz), 4.25 (t, 2H, J = 6.4 Hz), 2.21-2.14 (m, 1H), 1.51-1.32 (m, 8H), 1.00 (t, 3H, J = 7.4 Hz), 0.95 (t, 3H, J = 7.2 Hz). ^{13}C NMR (400 MHz, $CDCl_3$-d_6, δ, m.d.): 141.45, 140.14, 138.55, 133.28, 125.95, 125.86, 125.71, 125.56, 124.00, 123.61, 123.40, 123.07, 120.46, 119.52, 118.91, 118.80, 110.84, 110.77, 109.25, 109.15, 47.57, 39.52, 31.09, 28.91, 24.48, 23.14, 14.13, 10.99. MS (APCI$^+$, 20 V): 444.67 ([M+H], 100%).

Preprints (www.preprints.org) | NOT PEER-REVIEWED | Posted: 9 November 2023 doi:10.20944/preprints202311.0596.v1

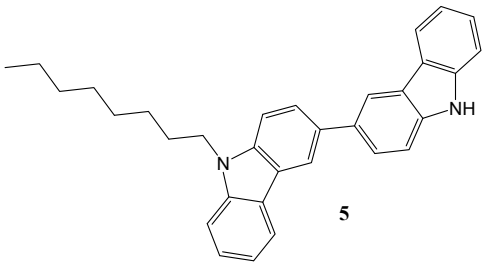

5

9-Octyl-9′H-3,3′-bicarbazole (**5**). 1-Bromooctane (1.16 g, 6.02 mmol) was added to a stirred solution of 3,3′-bicarbazole (**2**) (2.00 g, 6.02 mmol) in 50 ml of tetrahydrofuran. The mixture was heated to reflux, then potassium carbonate (1.66 g, 12.04 mmol) and powdered potassium hydroxide (2.02 g, 36.12 mmol) was added stepwise. The resulting mixture was left to react for 4h. After TLC control, the inorganic salts were filtered off and the product was purified by silica gel column chromatography using tetrahydrofuran/hexane (vol. ratio 1:7) as an eluent. Yield: 1.15 g (43%) of yellowish material. ^{1}H NMR (400 MHz, $CDCl_3$-d_6, δ, m.d.): 8.45 (d, 2H, J = 8.0 Hz), 8.25-8.20 (m, 2H), 8.04 (s, 1H), 7.87 (d, 1H, J = 8.0 Hz), 7.83 (dd, 1H, J_1 = 8.4 Hz, J_2 = 1.6 Hz), 7.56-7.50 (m, 3H), 7.48 (d, 3H, J = 7.2 Hz), 7.31 (t, 2H, J = 8.0 Hz), 4.37 (t, 2H, J = 7.0 Hz), 1.95 (qu, 2H, J = 7.3 Hz), 1.48-1.30 (m, 10H), 0.92 (t, 3H, J = 7.0 Hz). ^{13}C NMR (400 MHz, $CDCl_3$-d_6, δ, m.d.): 140.94, 140.02, 139.62, 138.53, 133.30, 125.94, 125.85, 125.70, 125.56, 124.00, 123.61, 123.42, 123.08, 120.49, 120.45, 120.40, 119.51, 119.00, 118.92, 118.79, 110.80, 110.74, 108.92, 108.83, 43.25, 31.85, 29.45, 29.23, 29.08, 27.39, 22.65, 14.12. MS (APCI$^+$, 20 V): 444.67 ([M+H], 100%).

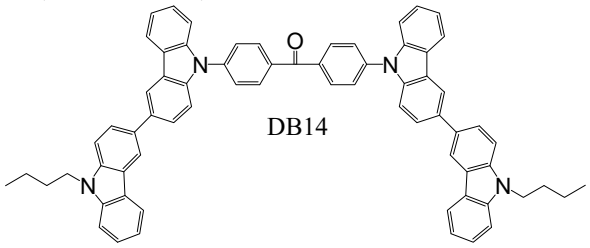

DB14

4,4′-Bis(9′-butyl-[3,3′]-bicarbazol-9-yl)benzophenone (**DB14**). 9-Butyl-9′H-3,3′-bicarbazole (**3**) (0.40 g, 1.03 mmol) and sodium hydride (0.10 g, 4.12 mmol) were stirred in 6 ml of DMF at room temperature under nitrogen for 20 min. Then, 4,4′-difluorobenzophenone (0.110 g, 0.515 mmol) was added to the reaction and resulting mixture was stirred at 150 °C under nitrogen for 4 h. After TLC control the reaction mixture was cooled and quenched by the addition of ice water. The product was extracted by chloroform. The combined extract was dried over anhydrous Na_2SO_4. The crude product was purified by silica gel column chromatography using the mixture of THF and hexane (vol. ratio 1:3) as an eluent. Yield: 0.38 g (77%) of yellow amorphous material. T_g = 145 °C (DSC). ^{1}H NMR (400 MHz, $CDCl_3$-d_6, δ, m.d.): 8.51-8.41 (m, 4H), 8.30-8.23 (m, 6H), 7.91-7.83 (m, 8H), 7.71 (d, 2H, J = 8.4 Hz), 7.65 (d, 2H, J = 8.4 Hz), 7.57-7.38 (m, 10H), 7.32-7.29 (m, 4H), 4.42-4.36 (m, 4H), 1.98-1.91 (m, 4H), 1.51-1.45 (m, 4H), 1.01 (t, 6H, J = 7.4 Hz). MS (APCI$^+$, 20 V): 954.8 ([M+H], 100%).

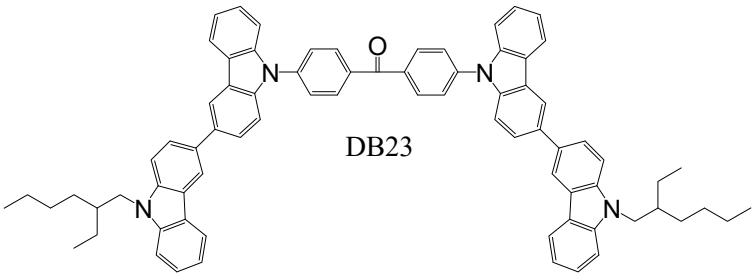

DB23

 doi:10.20944/preprints202311.0596.v1

4,4′-Bis(9′-{2-ethylhexyl}-[3,3′]-bicarbazol-9-yl)benzophenone (**DB23**). 9-[2-Ethylhexyl]-9′H-3,3′-bicarbazole (**4**) (0.40 g, 0.90 mmol) and sodium hydride (0.10 g, 4.12 mmol) were stirred in 6 ml of DMF at room temperature under nitrogen for 20 min. Then, 4,4′-difluorobenzophenone (0.100 g, 0.45 mmol) was added to the reaction and resulting mixture was stirred at 150 °C under nitrogen for 4 h. After TLC control the reaction mixture was cooled and quenched by the addition of ice water. The product was extracted by chloroform. The combined extract was dried over anhydrous Na_2SO_4. The crude product was purified by silica gel column chromatography using the mixture of THF and hexane (vol. ratio 1:5) as an eluent. Yield: 0.40 g (83%) of yellow amorphous material. T_g = 104 °C (DSC). ^{1}H NMR (400 MHz, $CDCl_3$-d_6, δ, m.d.): 8.51-8.45 (m, 4H), 8.31-8.22 (m, 6H), 7.91-7.79 (m, 8H), 7.76-7.70 (m, 4H), 7.66-7.36 (m, 14H), 4.27-4.23 (m, 4H), 1.90-1.87 (m, 2H), 1.47-1.29 (m, 16H), 1.00-0.90 (m, 12H). ^{13}C NMR (400 MHz, $CDCl_3$-d_6, δ, m.d.): 195.67, 141.42, 140.70, 140.22, 135.79, 132.79, 131.96, 129.44, 128.17, 127.18, 126.36, 126.13, 125.75, 125.49, 125.45, 124.56, 124.19, 123.42, 122.98, 120.77, 120.41, 119.02, 118.92, 118.82, 118.77, 110.08, 109.95, 109.27, 109.13, 47.57, 39.50, 31.06, 28.89, 24.45, 23.10, 14.09, 10.96. MS (APCI$^+$, 20 V): 1066.55 ([M+H], 100%).

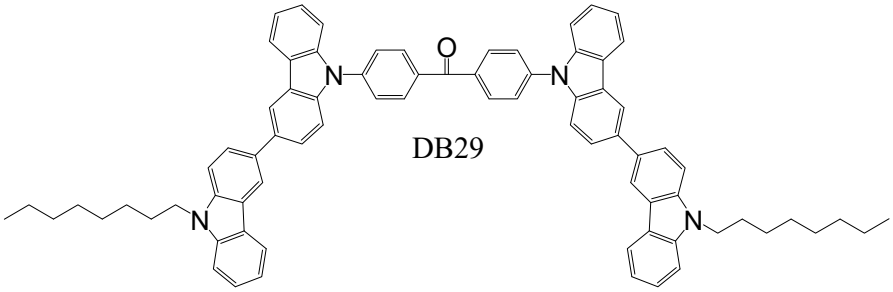

DB29

4,4′-Bis(9′-octyl-[3,3′]-bicarbazol-9-yl)benzophenone (**DB29**). 9-Octyl-9′H-3,3′-bicarbazole (**5**) (0.40 g, 0.90 mmol) and sodium hydride (0.10 g, 4.12 mmol) were stirred in 6 ml of DMF at room temperature under nitrogen for 20 min. Then, 4,4′-difluorobenzophenone (0.100 g, 0.45 mmol) was added to the reaction and resulting mixture was stirred at 150 °C under nitrogen for 4 h. After TLC control the reaction mixture was cooled and quenched by the addition of ice water. The product was extracted by chloroform. The combined extract was dried over anhydrous Na_2SO_4. The crude product was purified by silica gel column chromatography using the mixture of THF and hexane (vol. ratio 1:5) as an eluent. Yield: 0.44 g (92%) of yellow amorphous material. T_g = 95 °C (DSC). ^{1}H NMR (400 MHz, $CDCl_3$-d_6, δ, m.d.): 8.50 (dd, 4H, J_1 = 15.2 Hz, J_2 = 1.6 Hz), 8.30 (d, 2H, J = 7.6 Hz), 8.27-8.24 (m, 6H), 7.91-7.86 (m, 8H), 7.71 (d, 2H, J = 8.4 Hz), 7.66 (d, 2H, J = 8.0 Hz), 7.56-7.47 (m, 8H), 7.42 (t, 2H, J = 7.2 Hz), 7.33-7.29 (m, 2H), 4.38 (t, 4H, J = 7.2 Hz), 1.99-1.92 (m, 4H), 1.48-1.30 (m, 20H), 0.92 (t, 6H, J = 6.6 Hz). ^{13}C NMR (400 MHz, $CDCl_3$-d_6, δ, m.d.): 194.51, 142.04, 140.96, 140.71, 139.74, 139.28, 135.78, 135.41, 132.84, 131.97, 126.38, 126.34, 126.15, 125.79, 125.49, 124.57, 124.20, 123.48, 123.03, 120.78, 120.66, 120.50, 119.02, 118.85, 110.09, 109.97, 109.00, 108.87, 43.26, 31.85, 29.45, 29.23, 29.08, 27.39, 22.65, 14.12. MS (APCI$^+$, 20 V): 1067.78 ([M+H], 100%).

2.3. Device Fabrication

OLED devices were fabricated utilizing a pre-sputtered ITO glass substrate. The substrate underwent a thorough cleaning process, including 30-minute treatments with acetone and isopropyl alcohol (IPA) at elevated temperatures of 50 and 60 °C. Subsequently, the substrates were transferred to a UV chamber that was preheated and exposed to UV light for 10 minutes. The deposition of layers occurred within a glove box, maintaining an inert atmosphere. The hole injection layer (PEDOT:PSS) was spin-coated onto the substrates for 20 seconds at 4000 rpm, followed by a 10-minute heating step at 130 °C. Subsequently, the cooled substrates were subjected to a 20-second spin-coating process at 2500 rpm for the emissive layer. The subsequent stages encompassed thermal evaporation of the electron-injecting/transporting layer and aluminum cathode within a vacuum of 10^{-6} torr. The substrates remained under vacuum conditions within a mini chamber in the glove box to preserve

Preprints (www.preprints.org) | NOT PEER-REVIEWED | Posted: 9 November 2023 doi:10.20944/preprints202311.0596.v1

their quality until individual testing. All testing protocols were executed in a completely dark environment under ambient conditions. The CS-100A luminescence spectrophotometer was employed for recording the current-density–voltage–luminance (J-V-L) characteristics, while the PR-655 spectrophotometer was used for power efficacy–luminance–current characteristics. A Keithley voltmeter was utilized to measure the current-voltage (I-V) characteristics. The device area was determined to be 0.09 cm^2. The EQE of the devices was computed following the methodology outlined in the relevant literature, meticulously adhering to this approach during the testing and analysis procedures [20].

3. Result and Discussion

A three-step synthetic pathway was employed to synthesize the bicarbazole-based materials as it is demonstrated in Scheme 1.

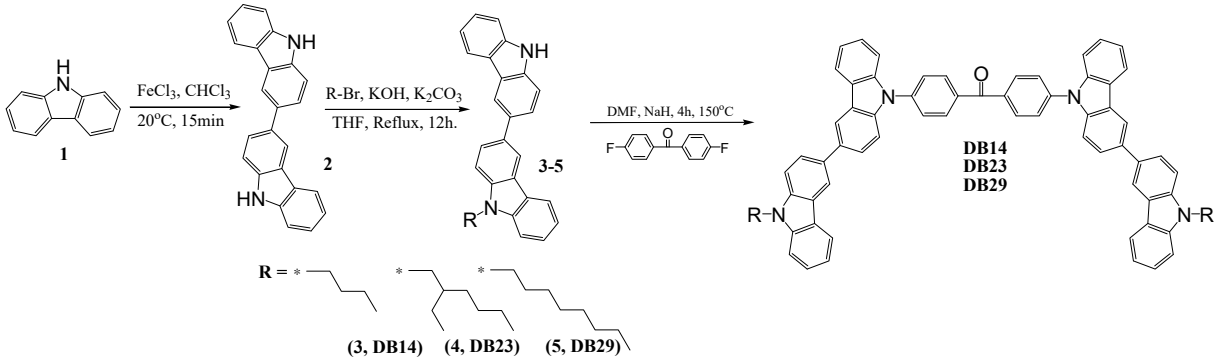

Scheme 1. Synthetic pathway of the derivatives DB14, DB23 and DB29.

3,3'-Bicarbazole (2) was synthesized through the oxidation of 9H-carbazole (1) using iron (III) chloride. Various 9-alkyl-9'H-3,3'-bicarbazoles (3-5) were prepared via N-alkylation reactions between a bicarbazole and corresponding alkyl bromides, utilizing potassium hydroxide and potassium carbonate in tetrahydrofuran (THF). The next step involved nucleophilic aromatic substitution of partially alkylated bicarbazole with 4,4'-difluorobenzophenone. This reaction was conducted in DMF, employing sodium hydride as a base, yielding the desired materials. This multi-step process resulted in the successful synthesis of the targeted bicarbazole-based compounds. In Figure 1, the chemical structures of DB14, DB23 and DB29 derivatives are presented, arranged based on the ascending order of their alkyl chain lengths. Values of glass transition temperatures (T_g), which depend also on the different alkyl chains, are also presented in the Figure 1.

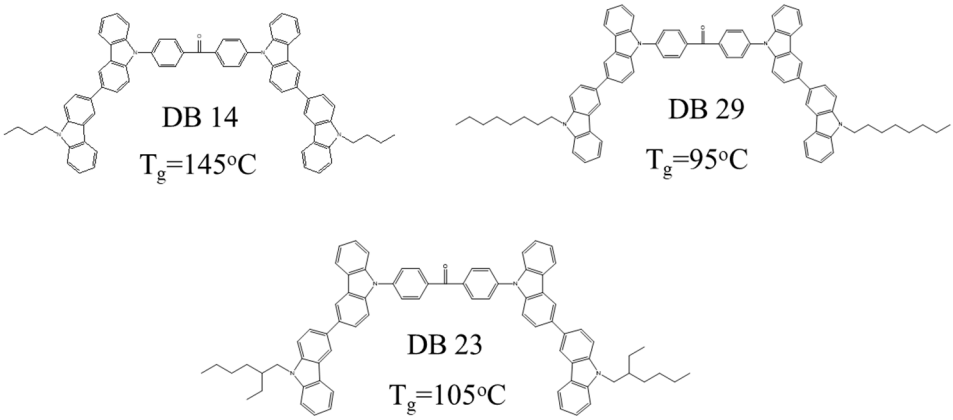

Figure 1. Chemical structures of the bicarbazole-benzophenone-based twisted D-A-D derivatives DB 14, DB 23 and DB 29.

3.1. Material Characteristics

Preprints (www.preprints.org) | NOT PEER-REVIEWED | Posted: 9 November 2023 doi:10.20944/preprints202311.0596.v1

3.1.1. DFT Calculations

The compounds DB14, DB23 and DB29 have the electron density contours of frontier molecular orbitals (FMO) namely the highest occupied molecular orbital (HOMO) and lowest unoccupied molecular orbital (LUMO) and singlet, triplet, and singlet-triplet energy gap electron distribution, which are recorded in Table 1 and Figure 2. Theoretical measurements of DB14, DB23 and DB29 compounds reveal their HOMO and LUMO levels, as well as the energy gap differentiating singlet and triplet states (ΔE_{ST}), alongside singlet and triplet energies. In all cases, these materials exhibit a narrow ΔE_{ST} (<0.15 eV), indicating efficient harnessing of triplet-level excitons. The HOMO and LUMO energy levels are suitable to the advancement of blue OLEDs and establish their potential as emitting materials for OLED devices.

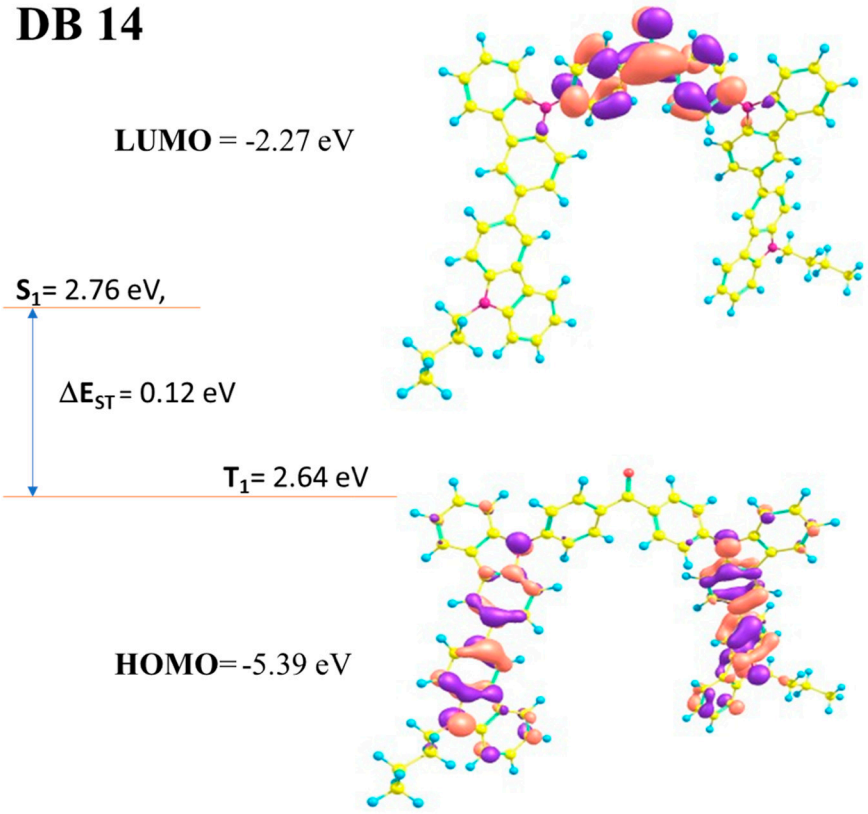

Preprints (www.preprints.org) | NOT PEER-REVIEWED | Posted: 9 November 2023 doi:10.20944/preprints202311.0596.v1

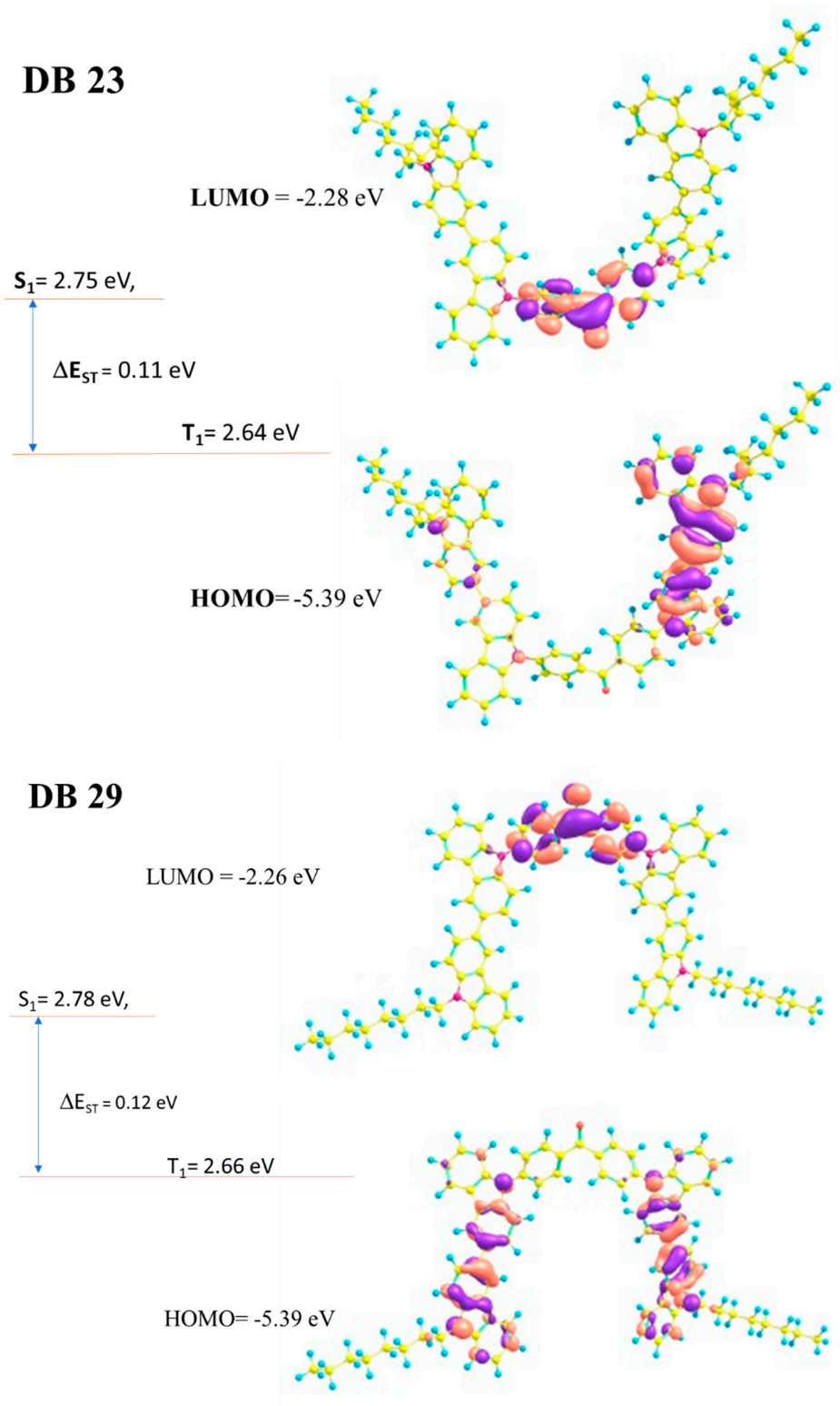

Figure 2. Electron density contours of FMO and HOMO, LUMO, singlet, triplet, and singlet-triplet energy gap electron distribution of the compounds DB 14, DB 23 and DB 29.

3.1.2. Photophysical Properties

The compounds DB14, DB23 and DB29 exhibit substantial photoluminescence quantum yields (PLQY) of 55.6, 52.0 and 55.5%, respectively. The values of PLQY are summarized in Table 1. The UV-absorption bands of these compounds are demonstrated in Figure 3. The materials were investigated using tetrahydrofuran (THF) solvent under typical conditions. Notably, all the compounds displayed

Preprints (www.preprints.org) | NOT PEER-REVIEWED | Posted: 9 November 2023 doi:10.20944/preprints202311.0596.v1

primary and secondary absorption peaks consistently at around 375 and 400 nm. The UV absorption wavelength and intensity were also used to construct the tauc plots for the materials (Figure 3) using the following values: $(\alpha \times h\nu)^{1/2}$ for x-axis and $h\nu$ for y-axis, where α is the intensity and $h\nu$ is the energy ($h\nu$ = 1240/wavelength). The tauc plots demonstrated bandgaps of the investigated compounds, which are 3.05 eV for DB14, 3.08 eV for DB 23 and 3.02 eV for DB 29 (Table 1).

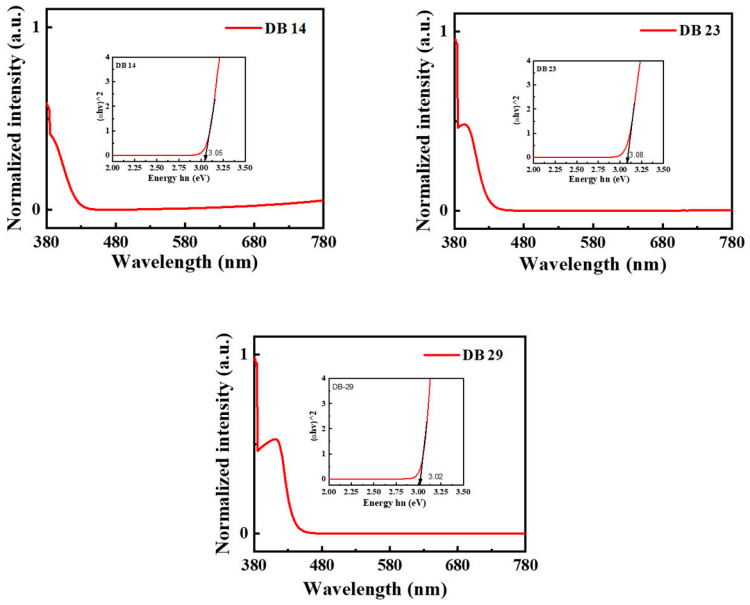

Figure 3. Ultraviolet-visible absorbance spectra and tauc plots (inset) of the compounds DB14, DB23 and DB29.

For the measurements of photoluminescence, the maxima absorbance wavelengths, which are presented in Table 1, were employed as the excitation wavelengths. In Figure 4, the photoluminescence (PL) spectra of the derivatives DB14, DB23 and DB29 are depicted. They show very similar emission bands for all the compounds with maxima wavelengths of approximately 400 nm due to similar electronic structure of the derivatives.

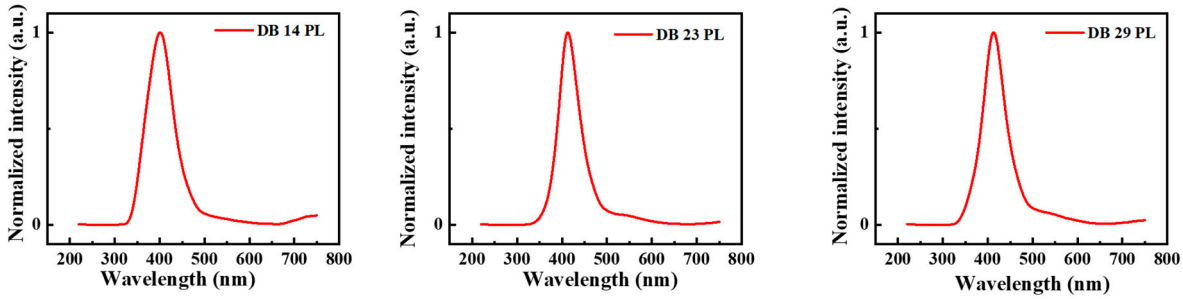

Figure 4. Photoluminescence (PL) spectra of the compounds DB14, DB23 and DB29.

Moreover, in order to determine the triplet energies of the potential emitters, low-temperature photoluminescence (LTPL) spectra were recorded. Notably, the compounds DB14, DB23 and DB29 exhibit elevated triplet energy levels of 2.83, 2.84 and 2.73 eV, respectively, as visually represented in Figure 5. These specific

Preprints (www.preprints.org) | NOT PEER-REVIEWED | Posted: 9 November 2023 doi:10.20944/preprints202311.0596.v1

characteristics are also included in Table 1 for reference.

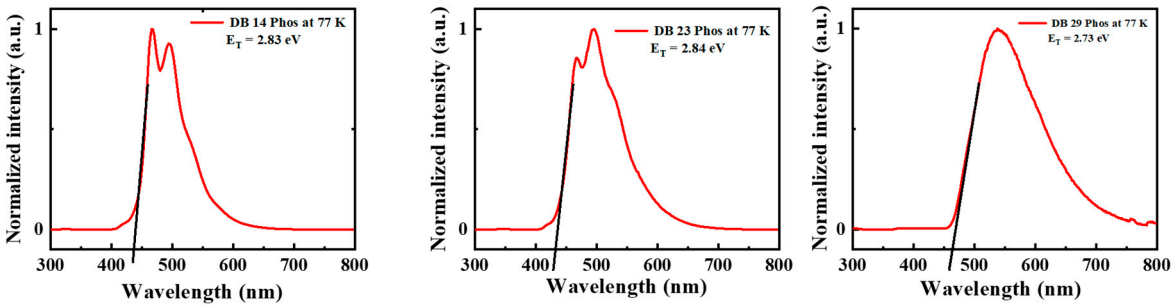

Figure 5. Low-temperature photoluminescence (LTPL) spectra at 77K of the compounds DB14, DB23 and DB29.

In Figure 6, the time-resolved photoluminescence (TRPL) analysis illustrates values of the decay times for DB14, DB23 and DB29 compounds, which were 3.40, 2.67 and 3.57 ns, respectively. It could be stated that all the lifetime curves of **the materials** present demonstarte only a nanosecond-scale component.

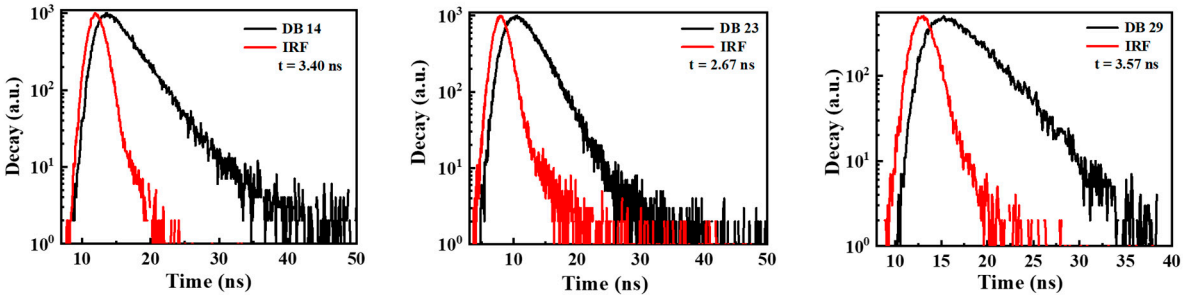

Figure 6. Time-resolved photoluminescence (TRPL) spectra for transient decay of the compounds DB14, DB23 and DB29.

3.1.3. Electrochemical Properties

The electrochemical attributes of DB 14, DB 23 and DB 29 compounds were assessed through cyclic voltammetry (CV) measurements, which are depicted in Figure 7. By using the obtained oxidation onset values the HOMO levels were calculated using the equation (1) and the LUMO levels were calculated by using the equation (2) [16]:

$$(1)\ \mathbf{E_{HOMO}} = -[4.4 + E^{ox}_{onset}]$$

$$(1)\ \mathbf{E_{LUMO}} = \mathbf{E_{HOMO}} + \mathbf{E_g}$$

The computed HOMO levels were -5.70, -5.63 and -5.66 eV, while the corresponding LUMO levels were -2.65, -2.55 and -2.64 eV for DB 14, DB 23 and DB 29 compounds, respectively. These values along with the earlier bandgap measurements are presented in Table 1. It could be stated that the HOMO and LUMO levels of the derivatives were found to be suitable as for blue emitters using the earlier mentioned CBP host material.

Preprints (www.preprints.org) | NOT PEER-REVIEWED | Posted: 9 November 2023 doi:10.20944/preprints202311.0596.v1

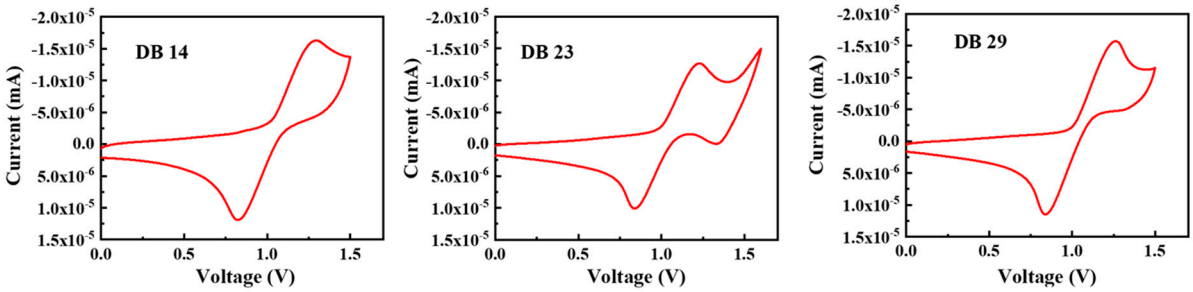

Figure 7. Cyclic voltammetry scans of the compounds DB14, DB23 and DB29.

2.1.4. Thermal Properties

The characteristics of thermal stability of the materials DB14, DB23 and DB29 were examined in a nitrogen atmosphere. Curves of the thermo-gravimetric analysis (TGA) are presented in Figure 8. For DB 14 having the shortest alkyl chains, the temperature at which 5% weight loss occurred, i.e. decomposition temperature (T_d), was obtained at 462 °C during heating. The materials DB23 and DB29, featuring lengthier aliphatic substitutions, exhibited lower thermal stability with T_d values of 383 °C and 384 °C, respectively. These findings demonstrate that the new materials have very good thermal stability as for emitting materials for application in OLED devices.

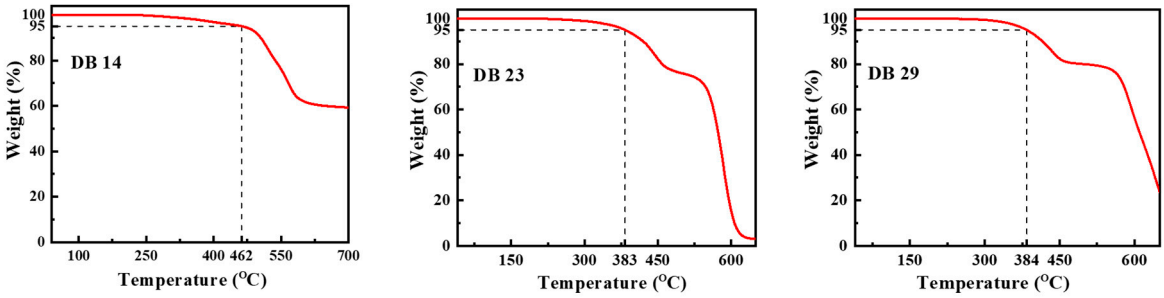

Figure 8. Curves of the thermo-gravimetric analysis (TGA) of the compounds DB14, DB23 and DB29.

The DSC thermos-grams of second heating for DB14, DB23 and DB29 compounds are displayed in Figure 9. Notably, upon analyzing the second heating curves, it becomes evident that the novel derivatives exhibit glass transition temperatures (T_g) that directly correlate with the length of their alkyl substituents. For instance, DB14 material with the shortest butyl substitution has the highest glass transition temperature of 145 °C. This trend persists also for compounds featuring more extended alkyl groups: DB23 and DB29 derivatives with 2-ethylhexyl and octyl substitutions, respectively, display glass transition temperatures of 104 °C and 95 °C. In totality, the results obtained from both TGA and DSC analyses confirm the high suitability of these materials for application within amorphous electroactive layers of OLED devices. Comprehensive T_d and glass-transition temperature (T_g) values are compiled in Table 1.

Preprints (www.preprints.org) | NOT PEER-REVIEWED | Posted: 9 November 2023 doi:10.20944/preprints202311.0596.v1

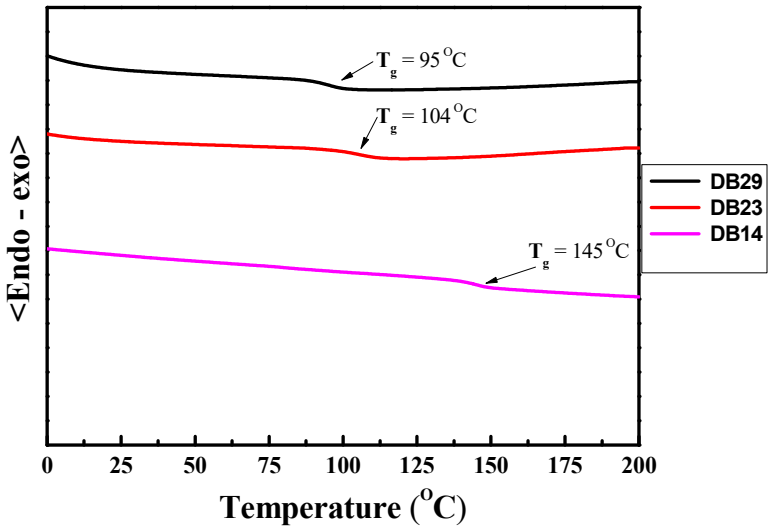

Figure 9. DSC thermo-grams of second heating of the compounds DB14, DB23 and DB29.

Table 1. Optoelectronic and thermal properties of the compounds DB14, DB23 and DB29.

Emitter	λ_{ex} (nm)	λ_{em} (nm)	E_g (eV)	Φ (%)	Decay (ns)	HOMO (eV)		LUMO (eV)		S_1 (eV)		T_1 (eV)		ΔE_{ST} (eV)		T_d (°C)	T_g (°C)
						Theo.	Cal.	Theo.	Cal.	Theo.	Cal.	Theo.	Cal.	Theo.	Cal.		
DB 14	366.7, 383.2	401.7	3.05	55.6	3.40	5.39	5.70	2.27	2.65	2.76	3.32	2.64	2.83	0.12	0.49	462	145
DB 23	380, 393.8	412.8	3.08	52.0	2.67	5.39	5.63	2.28	2.55	2.75	3.19	2.64	2.84	0.11	0.35	383	104
DB 29	382.7, 411.7	413.3	3.02	55.5	3.57	5.39	5.66	2.26	2.64	2.78	3.22	2.66	2.73	0.12	0.49	384	95

Λ_{ex} : Excitation Wavelength

Λ_{em} : Emission Wavelength

E_g : Bandgap

Φ : Photoluminescence Yield

S_1 : Singlet Energy

T_1 : Triplet Energy

ΔE_{ST} : Singlet-triplet Energygap

T_d : Decomposition Temperature

T_g : Glass Transition Temperature

Theo. : Theoretical Value

Cal. : Calculated Value

Preprints (www.preprints.org) | NOT PEER-REVIEWED | Posted: 9 November 2023 doi:10.20944/preprints202311.0596.v1

2.1.5. Electroluminescent Properties

The schematic energy level diagram in Figure 10 illustrates the configuration of blue OLED devices prepared in this study. These devices incorporated emitters DB14, DB23 and DB29, doped within a CBP host matrix. The device structure comprised of ITO/PEDOT:PSS/host CBP: emitter DB14, DB23 or DB29 (5, 10 or 15wt.%)/TPBi/LiF/Al.

The electroluminescence (EL) properties of the devices using the emitters doped within a CBP host matrix are shown in Figures 11-13. The corresponding characteristics for each emitter are also detailed in Table 2. Within each figure, various aspects are illustrated: (a) EL spectra, (b) current density-voltage characteristics, (c) luminance-voltage characteristics, (d) power efficacy-luminance characteristics, and (e) current efficacy-luminance characteristics.

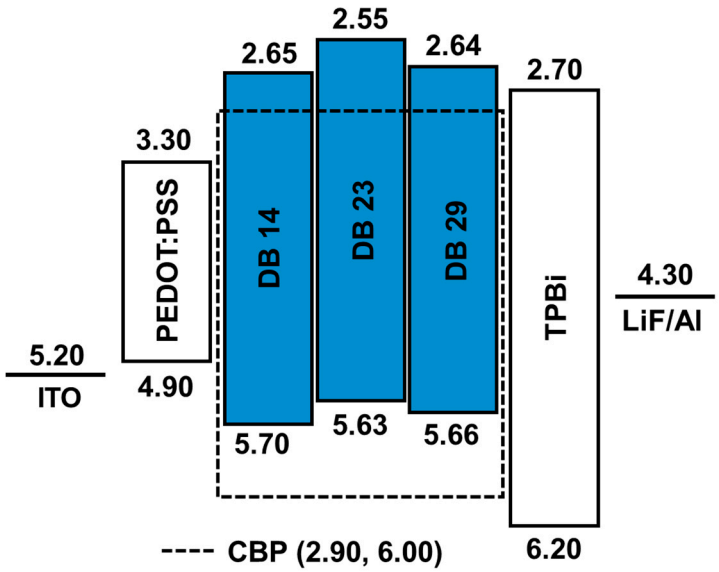

Figure 10. Energy-level diagram of the solution-processed blue OLED devices containing emitters DB14, DB23 and DB29 doped in a CBP host matrix.

In Figure 11(a), the EL spectra of device with DB14 exhibit a peak around 480 nm indicating blue emission. The presence of a sole peak implies successful host-guest energy transfer completion. The EL emission wavelength of the devices closely aligns with the PL spectra of emitter DB14 suggesting the source of emission. Notably, both doped and non-doped devices exhibit a similar EL emission peak. In Figures 11(b-e), the current density-luminance-voltage and power efficacy-luminance-current efficacy characteristics are depicted. The non-doped device exhibits significantly lower efficacy compared to the doped devices, highlighting the substantial role of the host material. Consequently, a device based on a 10 wt% doping concentration surpasses others in terms of power efficacy, showcasing a PE_{max} of 4.4 lm/W, CE_{max} of 7.6 cd/A, EQE_{max} of 3.3%, and L_{max} of 3175 cd/m² at a turn-on voltage of 5.1 V.

Preprints (www.preprints.org) | NOT PEER-REVIEWED | Posted: 9 November 2023 doi:10.20944/preprints202311.0596.v1

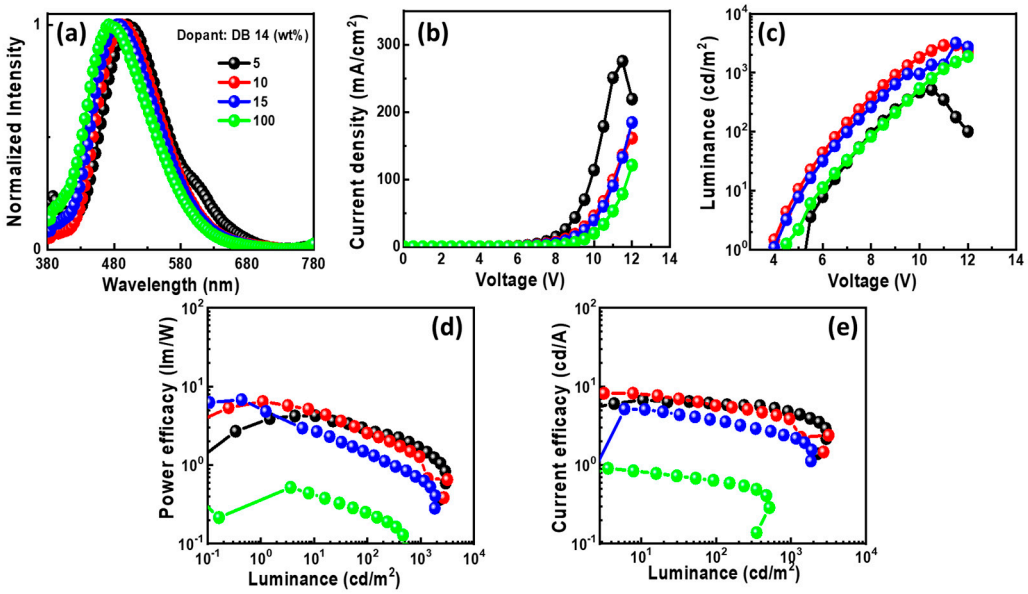

Figure 11. Electroluminescent (EL) properties of the devices using the emitter DB14 doped in CBP host matrix at varying concentrations showing (a) EL spectra, (b) current density-voltage, (c) luminance-voltage, (d) power efficacy-luminance, and (e) current efficacy-luminance characteristics.

In Figure 12(a) shown the EL spectra of the device with DB23 exhibit a single peak around 470 nm, indicating blue emission. Presence of the single peak suggests successful host-guest energy transfer completion. The EL emission wavelength of the devices closely matches the PL spectra of emitter DB23, confirming the origin of the emission. Notably, both doped and non-doped devices exhibit a similar EL emission peak. Figures 12(b-e) demonstrate current density-luminance-voltage and power efficacy-luminance-current efficacy characteristics. Comparatively, the non-doped device shows considerably lower efficacy than the doped devices demonstrating the crucial role of the host material. The device utilizing 15 wt% doping concentration of the emitter has a maxima PE_{max} of 3.2 lm/W, CE_{max} of 5.3 cd/A, and L_{max} of 2076 cd/m² at voltage of 5.1 V. Additionally, the device having 10 wt% doping concentration reveals a remarkable EQE_{max} of 5.3%, even surpassing the theoretical limit for fluorescent emitters. It is evident that the emitter DB23 based device stands out in comparison to the others.

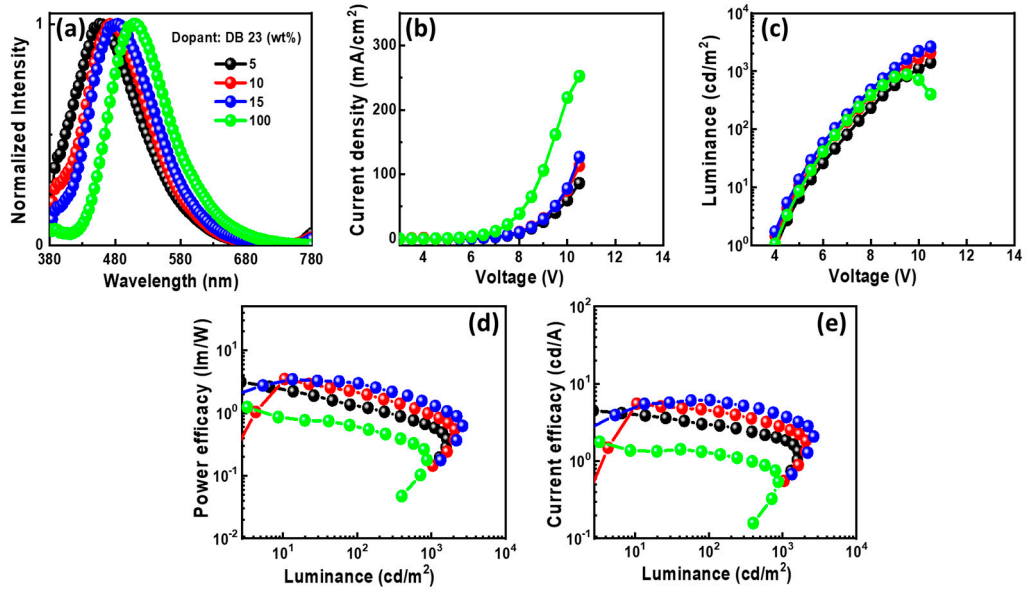

Preprints (www.preprints.org) | NOT PEER-REVIEWED | Posted: 9 November 2023 doi:10.20944/preprints202311.0596.v1

Figure 12. The electroluminescent (EL) properties of the device using emitter DB23 doped in CBP host matrix at varying concentrations: (a) EL spectra, (b) current density-voltage, (c) luminance-voltage, (d) power efficacy-luminance, and (e) current efficacy-luminance characteristics.

EL spectra of DB29 based device exhibit a blue shift with increasing doping concentration, in contrast to the non-doped device as it could be seen in Figure 13(a). The EL spectra maxima change from approximately 490 nm to 430 nm in region of blue emission. Single peaks of the emissions signify the achievement of complete host-guest energy transfer. Figures 13(b-e) illustrate the current density-luminance-voltage and power efficacy-luminance-current efficacy characteristics. The non-doped device showcases a more favorable current density-voltage characteristic compared to the doped devices, although its efficacy is considerably lower than that of the doped counterparts. Consequently, the role of the host material is pronounced, leading to the prominence of the device with a 15 wt% doping concentration. This device outperforms others in terms of power efficacy, exhibiting a PE_{max} of 7.9 lm/W, CE_{max} of 9.1 cd/A, EQE_{max} of 4.0%, and L_{max} of 2631 cd/m² voltage of 4.7 V. Impressively, this device showcases the highest PE and CE values among all.

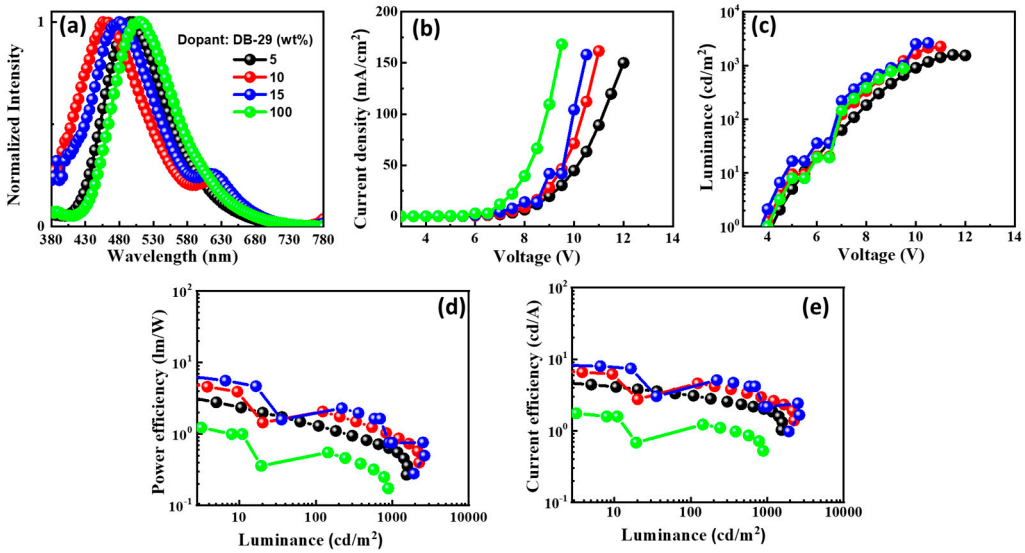

Figure 13. The electroluminescent (EL) properties of the device with emitter DB29 doped in CBP host matrix at varying concentrations: (a) EL spectra, (b) current density-voltage, (c) luminance-voltage, (d) power efficacy-luminance, and (e) current efficacy-luminance characteristics.

As depicted in Table 2, DB23 based device exhibits the highest EQE among all devices, surpassing both previous research and the outcomes of this study. This enhanced performance could be attributed to the inclusion of the branched alkyl sidechains in the molecule, which likely contributed to improved molecule solubility for the fabrication of wet-processed OLED devices and film forming properties of the material [17–19]. Nevertheless, concerning PE and CE DB29 based device demonstrated superior performance. This can be attributed to its appropriate HOMO and LUMO levels, which facilitated efficient host-guest energy transfer. Additionally, the incorporation of double bicarbazole donor moieties contributed to balanced charge transfer, further enhancing its performance.

Table 2. Electroluminescent (EL) characteristics of the devices with the emitters DB14, DB29 and DB23 doped in CBP host matrix at varying concentrations displaying turn-on voltage (V_{on}), power efficacy, current efficacy, external quantum efficiency (EQE), CIE and maximum luminance.

Emitter	Concentration of emitter in host material	Turn-on	Power efficacy (lm/W)	Current efficacy (cd/A)	EQE (%)	CIE

Preprints (www.preprints.org) | NOT PEER-REVIEWED | Posted: 9 November 2023 doi:10.20944/preprints202311.0596.v1

	(wt%)	Voltage (V_{on})[a]	@100/1,000 cd/m^2 and max				Max Luminance (cd/m^2)
DB-14	5.0	5.0	2.9/ 1.6/ 3.9	6.1/ 4.7/ 6.5	2.6/ 2.2/ 2.7	(0.22, 0.36)/ (0.21, 0.32)/ -	2951
	10	5.1	2.6/ 1.3/ 4.4	5.7/ 3.9/ 7.6	2.6/ 2.0/ 3.3	(0.21, 0.33)/ (0.20, 0.29)/ -	3175
	15	5.9	1.4/ 1.3/ 2.4	3.7/ 2.3/ 4.9	1.9/ 1.4/ 2.4	(0.20, 0.28)/ (0.19, 0.24)/ -	1884
	100	6.1	0.2/ -/ 0.4	0.6/ -/ 0.8	0.3/ -/ 0.4	(0.26, 0.40)/ -	515
DB-29	5.0	5.4	0.3/ 0.6/ 2.1	3.1/ 2.0/ 3.9	2.0/ 1.4/ 2.3	(0.19, 0.22)/ (0.22, 0.22)/ -	1578
	10	5.7	1.7/ 1.0/ 4.4	3.7/ 2.8/ 6.5	2.0/ 1.7/ 3.1	(0.20, 0.27)/ (0.23, 0.25)/ -	2251
	15	4.7	1.0/ 0.3/ 7.9	2.3/ 1.0/ 9.1	1.1/ 0.5/ 4.0	(0.21, 0.31)/ (0.22, 0.27)/ -	2631
	100	5.8	0.4/ -/ 1.4	0.8/ -/ 1.8	0.3/ -/ 0.7	(0.26, 0.44)/ -	884
DB-23	5.0	5.7	1.3/ 0.6/ 2.1	3.0/ 1.9/ 3.8	1.9/ 1.4/ 2.3	(0.17, 0.07)	883
	10	**5.2**	**1.4/ 0.8/ 1.7**	**2.4/ 1.7/ 2.6**	**5.1/ 3.5/ 5.3**	**(0.19, 0.22)/ (0.22, 0.22)/ -**	**1,620**
	15	5.2	2.2/ 1.0/ 3.2	4.6/ 2.8/ 5.3	2.5/ 1.7/ 2.7	(0.20, 0.27)/ (0.23, 0.25)/ -	2,076
	100	5.1	0.6/ -/ 1.0	1.3/ -/ 1.8	0.5/ -/ 0.7	(0.26, 0.44)/ -	875

[a] Turn-on voltage at luminance >1 cd m^{-2}.

4. Conclusions

In conclusion, this study presents a comprehensive exploration of twisted donor-acceptor-donor (D-A-D) derivatives, specifically bicarbazole-benzophenone-based compounds, as potential blue emitters for blue OLEDs. The synthesized emitters DB14, DB23 and DB29, were systematically designed with tailored alkyl side chains to enhance their film forming properties properties. The investigation encompassed thorough characterization, including photo-physical analysis to determine photoluminescence quantum yields, UV absorption, and emission characteristics. Electrochemical measurements provided insights into HOMO and LUMO energy levels, while thermal analysis unveiled the remarkable thermal stability of the compounds. OLED devices

incorporating these emitters demonstrated noteworthy performance with DB23 exhibiting the highest EQE among all devices reaching a peak value of 5.3%. The study also highlighted the significant influence of host-guest energy transfer, optimal doping concentrations and molecular structures on device efficiency. Notably, the research outcomes underscore the considerable potential of the newly developed D-A-D derivatives in advancing OLED technology. This work contributes to the ongoing progress of OLED materials and their applications, offering insights into the design of efficient blue emitters.

Author Contributions: Investigation, D.B., I.S., P.G., K.K., D.T. and G.K.; writing—original draft preparation, D.B., I.S., P.G. and S.B.; writing—review and editing, J.-H.J. and S.G. All authors have read and agreed to the published version of the manuscript.

Funding: This work was supported by the project funded by the Research Council of Lithuania (Grant No. S-MIP-22-84) and by the Ministry of Science and Technology (MOST), Taiwan (Grant No. 109-2923-M-007-003-MY3).

Data Availability Statement: The data presented in this study are available on request from the corresponding authors.

Acknowledgements: DT is thankful to the Lithuanian Academy of Sciences for support.

Conflict of Interest: There are no conflicts to declare.

References

1. Nakamura, S. Shuji Nakamura - Nobel Lecture: Background Story of the Invention of Efficient Blue InGaN Light Emitting Diodes. **2014**.
2. Blue LEDs-Filling the World with New Light.
3. Nobel Prize ® and the Nobel Prize ® Medal Design Mark Are Registrated Trademarks of the Nobel Foundation. **2014**.
4. Nayak, S.R.; Siddiqui, I.; Shahnawaz; Jou, J.-H.; Vaidyanathan, S. Diphenylimidazole Based Fluorophores for Explosive Chemosensors and as Efficient Host Materials for Green Phosphorescent Organic Light Emitting Diodes. *ACS Applied Optical Materials* **2022**, doi:10.1021/ACSAOM.2C00012.
5. Nayak, S.R.; Shahnawaz; Siddiqui, I.; Jou, J.H.; Patel, S.; Vaidyanathan, S. Multifunctional 4,5-Diphenyl-1 H-Imidazole-Based Luminogens as Near UV/Deep Blue Emitters/Hosts for Organic Light-Emitting Diodes and Selective Picric Acid Detection. *Journal of Physical Chemistry C* **2022**, doi:10.1021/ACS.JPCC.2C05220.
6. Gupta, N.; Nagar, M.R.; Anamika; Gautam, P.; Maiti, B.; Jou, J.H.; Kuila, B.K. Triazine and Thiophene-Containing Conjugated Polymer Network Emitter-Based Solution-Processable Stable Blue Organic LEDs. *ACS Appl Polym Mater* **2022**, doi:10.1021/ACSAPM.2C01337.
7. Solanki, J.D.; Siddiqui, I.; Gautam, P.; Gupta, V.K.; Jou, J.H.; Surati, K.R. Blue Fluorescent Zinc(II) Complexes Bearing Schiff Base Ligand for Solution-Processed Organic Light-Emitting Diodes with CIEy ≤ 0.09. *Opt Mater (Amst)* **2022**, *134*, doi:10.1016/j.optmat.2022.113222.
8. OLED Displays and Their Applications | Learning Corner for Beginners Available online: https://www.electronicsforu.com/resources/oled-displays-applications (accessed on 2 May 2022).
9. Siddiqui, I.; Kumar, S.; Tsai, Y.-F.; Gautam, P.; Shahnawaz; Kesavan, K.; Lin, J.-T.; Khai, L.; Chou, K.-H.; Choudhury, A.; et al. Status and Challenges of Blue OLEDs: A Review. *Nanomaterials* **2023**, *13*, 2521, doi:10.3390/NANO13182521/S1.
10. Bommireddy, P.R.; Musalikunta, C.S.; Lee, Y.-W.; Suh, Y.; Godumala, M.; Park, S.-H. Recent Endeavors and Perspectives in Developing Solution-Processable Host Materials for Thermally Activated Delayed Fluorescence Organic Light-Emitting Diodes. *J Mater Chem C Mater* **2023**, *11*, 13603–13624, doi:10.1039/D3TC02794E.
11. Gu, J.; Shi, W.; Zheng, H.; Chen, G.; Wei, B.; Wong, W.Y. The Novel Organic Emitters for High-Performance Narrow-Band Deep Blue OLEDs. *Topics in Current Chemistry 2023 381:5* **2023**, *381*, 1–38, doi:10.1007/S41061-023-00436-7.
12. Kim, H.S.; Cheon, H.J.; Lee, D.; Lee, W.; Kim, J.; Kim, Y.H.; Yoo, S. Toward Highly Efficient Deep-Blue OLEDs: Tailoring the Multiresonance-Induced TADF Molecules for Suppressed Excimer Formation and near-Unity Horizontal Dipole Ratio. *Sci Adv* **2023**, *9*, doi:10.1126/SCIADV.ADF1388/SUPPL_FILE/SCIADV.ADF1388_SM.PDF.

13. Wu, S.; Zhang, L.; Wang, J.; Kumar Gupta, A.; Samuel, I.D.W.; Zysman-Colman, E. Merging Boron and Carbonyl Based MR-TADF Emitter Designs to Achieve High Performance Pure Blue OLEDs**. *Angewandte Chemie International Edition* **2023**, *62*, e202305182, doi:10.1002/ANIE.202305182.
14. Mubarok, H.; Amin, A.; Lee, T.; Jung, J.; Lee, J.-H.; Lee, M.H. Triptycene-Fused Sterically Shielded Multi-Resonance TADF Emitter Enables High-Efficiency Deep Blue OLEDs with Reduced Dexter Energy Transfer. *Angewandte Chemie* **2023**, *135*, e202306879, doi:10.1002/ANGE.202306879.
15. Gautam, P.; Shahnawaz; Siddiqui, I.; Blazevicius, D.; Krucaite, G.; Tavgeniene, D.; Jou, J.H.; Grigalevicius, S. Bifunctional Bicarbazole-Benzophenone-Based Twisted Donor–Acceptor–Donor Derivatives for Deep-Blue and Green OLEDs. *Nanomaterials* **2023**, *13*, 1408, doi:10.3390/NANO13081408/S1.
16. Arnaboldi, S.; Benincori, T.; Mussini, P.R.; Beresneviciute, R.; Gautam, P.; Ram Nagar, M.; Krucaite, G.; Tavgeniene, D.; Jou, J.-H.; Grigalevicius, S. Naphtalimide-Based Bipolar Derivatives Enabling High-Efficiency OLEDs. *Molecules 2023, Vol. 28, Page 6027* **2023**, *28*, 6027, doi:10.3390/MOLECULES28166027.
17. (PDF) Synthesis of Side-Chain Polystyrenes for All Organic Solution Processed OLEDs Available online: https://www.researchgate.net/publication/318529009_Synthesis_of_side-chain_polystyrenes_for_all_organic_solution_processed_OLEDs (accessed on 30 June 2022).
18. Peng, F.; Zhong, W.; He, J.; Zhong, Z.; Guo, T.; Ying, L. Effect of Alkyl Side Chain Length on the Electroluminescent Performance of Blue Light-Emitting Poly(Fluorene-Co-Dibenzothiophene-S,S-Dioxide). *Dyes and Pigments* **2021**, *187*, 109139, doi:10.1016/J.DYEPIG.2021.109139.
19. Lee, T.; Song, C.E.; Lee, S.K.; Shin, W.S.; Lim, E. Alkyl-Side-Chain Engineering of Nonfused Nonfullerene Acceptors with Simultaneously Improved Material Solubility and Device Performance for Organic Solar Cells. *ACS Omega* **2021**, *6*, 4562–4573, doi:10.1021/ACSOMEGA.0C04495/ASSET/IMAGES/LARGE/AO0C04495_0007.JPEG.
20. De, D.; Pereira, S.; Data, P.; Monkman, A.; Pereira, S.; Monkman, A.P. Methods of Analysis of Organic Light Emitting Diodes. *researchgate.net 2*, 323–337.